

Role of a high ground-state centrifugal barrier in the breakup of the ^{31}Ne nucleus

B. Mukeru^{1†}

¹Department of Physics, University of South Africa, P. O. Box 392, Pretoria 003, South Africa

Abstract: An analysis of the breakup of the ^{31}Ne weakly-bound neutron-halo system on a lead target is presented, considering the $2p_{3/2}$ and $1f_{7/2}$ ground-state configurations. It is shown that a high centrifugal barrier almost wipes out the breakup channel, thus assimilating the breakup of a weakly-bound system to that of a tightly-bound system, and also reduces the range of the monopole nuclear potential. Consequently, a high centrifugal barrier prevents the suppression of the Coulomb-nuclear interference (CNI) peak by weakening couplings to the breakup channel and reducing the range of the monopole nuclear potential, two main factors that would otherwise suppress such a peak. The present study also identifies couplings to the breakup channel and a long-ranged monopole nuclear potential as the main factors that lead to the suppression of the CNI peak. A low centrifugal barrier together with a Coulomb barrier would also effectively prevent the suppression of the CNI peak in proton-halos as reported in the case of the ^8B proton-halo.

Keywords: centrifugal barrier, Coulomb-nuclear interference peak, elastic scattering cross section

DOI: 10.1088/1674-1137/ac9e4b

I. INTRODUCTION

Weakly-bound halo nuclei are a subject of current interest in physics. Since early studies of these systems [1], this field, once dominated by light weakly-bound halo systems as exemplified by several recent studies (Refs. [2–34]) on the breakup dynamics of these systems, has witnessed increasing identification of weakly-bound heavy neutron-halo systems, such as ^{31}Ne and ^{37}Mg [35–45], located on the neutron-rich limit of the nuclear chart. Owing to the effect of the centrifugal barrier, halo features are manifest in low ($\ell = 0, 1$) orbital angular momenta [46]. However, a better understanding of how a large orbital angular momentum hinders the manifestation of halo features in breakup reactions could be interesting. Such study could be helpful because it may serve to predict whether future halo structures in higher partial-waves are possible by investigating how this parameter influences the breakup process of a weakly-bound projectile.

Although the standard shell model predicts the ground-state of the ^{31}Ne nucleus to be in the f-state ($1f_{7/2}$) [43, 47–49], experimental and theoretical studies have identified this nucleus as a neutron-halo system in the $2p_{3/2}$ ground-state [41–43, 45]. By studying the breakup of ^{31}Ne through both the $2p_{3/2}$ and $1f_{7/2}$ ground-states [44], it has been shown that the latter ($1f_{7/2}$) does

not describe the features of breakup reactions induced by weakly-bound projectiles, such as a narrow parallel momentum distributions (see Fig. 10 of that reference and the related text). The study in Ref. [44] did not consider other reaction channels, such as elastic scattering, where the projectile halo features are also manifested. Even though a $1f_{7/2}$ ground-state does not describe the halo structure of this nucleus, it provides an opportunity to examine how a large orbital angular momentum inhibits the manifestation of halo features in breakup reactions.

In this paper, as in Ref. [44], we study the breakup of ^{31}Ne on a lead target, considering both the $2p_{3/2}$ and $1f_{7/2}$ ground-states. The main objective is to investigate how a high centrifugal barrier in the ground-state inhibits the manifestation of halo features in breakup processes. To this end, we assess (1) how it affects the Coulomb-nuclear interference (CNI) peak in the elastic scattering cross section, and (2) to what extent it suppresses the breakup channel. The origin of the suppression of the CNI peak in elastic scattering is yet to be clarified. For example, in Ref. [12], the CNI peak in the elastic scattering cross section is suppressed in the breakup of the ^{11}Be system on a lead target. However, in Ref. [14], a pronounced CNI peak is reported in the breakup of ^8B on the same target in the same incident energy range. Does this suggest that the suppression of the CNI peak may not necessarily be attributed to the coupling to the breakup

Received 5 September 2022; Accepted 28 October 2022

[†]E-mail: mukerb1@unisa.ac.za

©2023 Chinese Physical Society and the Institute of High Energy Physics of the Chinese Academy of Sciences and the Institute of Modern Physics of the Chinese Academy of Sciences and IOP Publishing Ltd

channel, as inferred in Refs. [12, 50, 51]? In Ref. [34], the suppression of the CNI peak is attributed to the polarization potential. We expect the present study to shed more light on this issue. Unlike in previous studies on the breakup of the ^{31}Ne nucleus at high incident energies, we consider an incident energy closer to the Coulomb barrier (twice as large as the Coulomb barrier). As for the ground-state separation energy of the ^{31}Ne system, there is still no consensus as yet because different measurements have reported different values: -0.06 ± 0.41 MeV [52], $-0.15^{+0.16}_{-0.1}$ MeV [42], -0.29 ± 1.64 MeV [53], and -0.30 ± 1.6 MeV [54], whereas the 2003 mass evaluation [55] reported a value of $S_n = -0.33$ MeV.

This paper is structured as follows: In Sec. II, the details of the numerical calculations and results are discussed, and the main results are presented in Sec. III.

II. NUMERICAL CALCULATIONS AND RESULTS

A. Numerical calculations

The fundamentals of the continuum discretized coupled-channels (CDCC) formalism, which is adopted in the present study, are available in literature, such as Refs. [56–58]. Therefore, we do not intend to repeat the details here. Only the different ingredients that are needed in the numerical solution of the CDCC coupled differential equations are described. The ^{31}Ne projectile nucleus is modeled as $^{31}\text{Ne} \rightarrow {}^{30}\text{Ne} + n$, where the valence neutron is weakly-bound to the core nucleus ${}^{30}\text{Ne}$. As already stated in the introduction, we consider the $2p_{3/2}$ and $1f_{7/2}$ ground-state configurations. Although the goal is not to investigate the role of the ground-state separation energy on the breakup observables, two different values, $S_n = -0.15$ MeV and $S_n = -0.33$ MeV, are considered. The parameters of the core-neutron Woods-Saxon potential used to generate the projectile bound and continuum states are $R_0 = R_{\text{SO}} = 3.946$ fm, $a_0 = a_{\text{SO}} = 0.67$ MeV, and $V_{\text{SO}} = -17.33$ MeV, taken from Ref. [45], where (R_0, a_0) are the radius and diffuseness of the central term, respectively, and $(V_{\text{SO}}, R_{\text{SO}}, a_{\text{SO}})$ are the depth, radius, and diffuseness of the spin-orbit coupling term, respectively. For the $2p_{3/2}$ ground-state, the depth of the central term V_0 is adjusted to $V_0 = -49.409$ MeV to obtain the ground-state binding energy $S_n = -0.15$ MeV and to $V_0 = -49.724$ MeV to obtain $S_n = -0.33$ MeV. For the $1f_{7/2}$ ground-state, V_0 is adjusted to $V_0 = -48.315$ MeV to obtain $S_n = -0.15$ MeV and to $V_0 = -48.98$ MeV to obtain $S_n = -0.33$ MeV. The core-target and neutron-target optical potentials are obtained from the global parameterization of Akyuz-Winther [59]. To account for the projectile halo structure in the elastic scattering channel, the monopole nuclear potential in this channel is calculated by folding the projectile ground-state wave function with

core-target and neutron-target interactions. For the numerical integration of the CDCC coupled differential equations, the maximum angular momentum between the core nucleus and the neutron is truncated by $\ell_{\max} = 5\hbar$, the maximum matching radius for bin integration by $r_{\max} = 150$ fm, the maximum order of the potential multipole expansion by $\lambda_{\max} = 5$, the maximum matching radius of the integration of the coupled differential equations by $R_{\max} = 1000$ fm, and the maximum angular momentum of the relative center-of-mass motion by $L_{\max} = 10000\hbar$. The projectile excitation energy up to $\varepsilon_{\max} = 10$ MeV is considered, with the $[0, \varepsilon_{\max}]$ interval sliced into energy bins of widths $\Delta\varepsilon = 0.5$ MeV for s -state and p -state, $\Delta\varepsilon = 1.0$ MeV for f -state and d -state, and $\Delta\varepsilon = 1.5$ MeV for higher-order partial-waves. The numerical calculations are carried out with Fresco code [60].

B. Results and discussion

We start with the densities of the ground-state wave functions $|u_{\ell_0}^{j_0}(r)|^2$, where ℓ_0 is the ground-state orbital angular momentum, j_0 is the ground-state total angular momentum, and r is the relative coordinate between the core nucleus and the valence neutron, which are shown in Fig. 1 for the $2p_{3/2}$ (panel (a)) and $1f_{7/2}$ (panel (b)) ground-states. A comparison of both panels shows, as expected, that the higher centrifugal barrier in the $1f_{7/2}$ state serves to suppress the longer tail of the wave function. Moreover, the gap between the two densities in panel (b) almost disappears, suggesting that a higher centrifugal barrier significantly suppresses the effect of the separation on the wave function. It is shown in Refs. [30, 31, 61, 62] that the centrifugal barrier prevents the wave function from extending to infinity in the $S_n \rightarrow 0$ limit.

Figure 2 shows the $2p_{3/2}$ and $1f_{7/2}$ elastic scattering cross sections calculated at an incident energy $E_{\text{lab}} =$

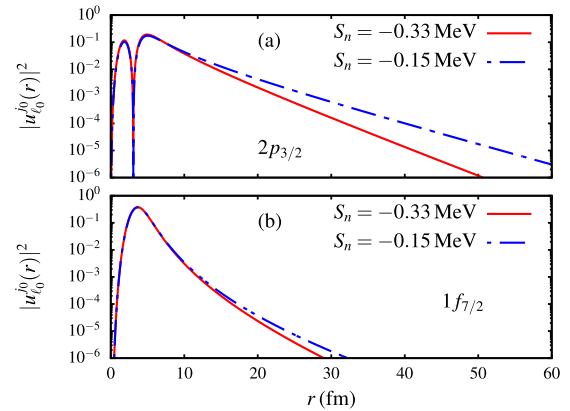


Fig. 1. (color online) Densities of the ground-state wave functions for both the $2p_{3/2}$ ground-state (panel (a)) and $1f_{7/2}$ ground-state (panel (b)), corresponding to $S_n = -0.33$ MeV and $S_n = -0.15$ MeV.

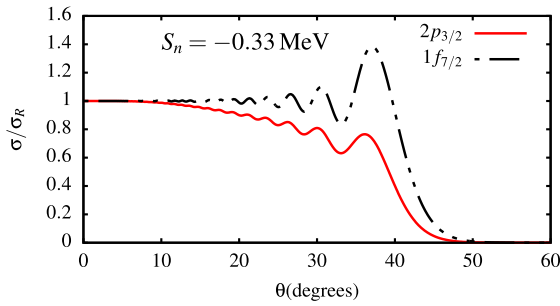


Fig. 2. (color online) Elastic scattering cross sections corresponding to the $2p_{3/2}$ and $1f_{7/2}$ ground-states, considering $S_n = -0.33$ MeV.

$2 \times V_B$, where $V_B = 89$ MeV is the Coulomb barrier height, and scaled by the Rutherford cross section. Comparing the two elastic scattering cross sections, one notices that the σ/σ_R ratio for $2p_{3/2}$ deviates earlier from unity with a non-existent CNI peak. The absence of this peak has also been observed in other weakly-bound neutron-halo projectiles, such as ^{37}Mg [27] and ^{11}Be [12, 50, 51]. An early deviation of the σ/σ_R ratio from unity signals the importance of the breakup channel, which is a characteristic of weakly-bound projectiles. However, for $1f_{7/2}$, the σ/σ_R ratio exhibits a different behavior in which a well pronounced CNI peak is noticed at approximately 40° , with a delayed deviation of this ratio from unity compared to that of $2p_{3/2}$. The late deviation from unity of this ratio for the $1f_{7/2}$ ground-state compared to that of the $2p_{3/2}$ ground-state is an indication of the lower importance of the breakup channel in the former case than in the latter. It follows that a high centrifugal barrier prevents the suppression of the CNI peak and undermines the relevance of the breakup channel in elastic scattering. To better make sense of this assertion, Fig. 3 displays the elastic scattering cross sections with couplings to the breakup channel (BU) and without couplings to the breakup channel, that is, there is no breakup of the projectile (No BU). In panel (a) ($2p_{3/2}$ ground-state), the "No BU" scattering cross section exhibits a pronounced CNI peak at approximately 40° , which is suppressed (by approximately 32 %) owing to the couplings to the breakup channel. Therefore, the fact that strong couplings to the breakup channel are responsible for the suppression of the CNI peak is asserted, for example, in Refs. [12, 50, 51]. However, panel (b) ($1f_{7/2}$ ground-state) shows that couplings to the breakup channel do not represent any meaningful effect on the CNI peak. This is because the breakup channel is weakened by a high centrifugal barrier in the ground-state. It follows that a high centrifugal barrier in the projectile ground-state restricts the significance of the breakup channel, which would otherwise serve to suppress the CNI peak in the elastic scattering cross section. This is also the main reason why no CNI suppression is reported in Ref. [14] in the breakup of the

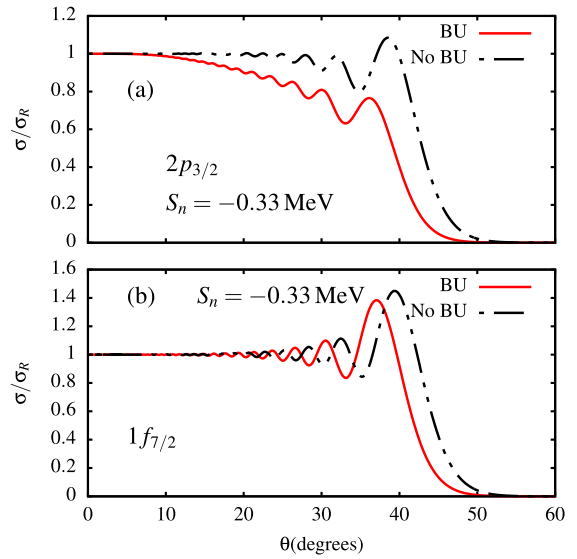


Fig. 3. (color online) Elastic scattering cross sections corresponding to the couplings to the breakup channel ("BU") and when there is no projectile breakup (no couplings to the breakup channel "No BU") corresponding to the $2p_{3/2}$ ground-state (panel (a)) and $1f_{7/2}$ ground-state (panel (b)) for $S_n = -0.33$ MeV.

^{8}B nucleus, which contains both Coulomb and centrifugal barriers in its ground-state.

Let us now assess the effect of the range of the monopole nuclear interaction on the CNI peak. As already indicated, the monopole nuclear potential is calculated by folding the projectile ground-state wave function with core-target and neutron-target interactions, meaning that it has a longer range for $2p_{3/2}$ than $1f_{7/2}$ according to Fig. 1. A careful observation of both panels (a) and (b) of Fig. 3 shows that the $1f_{7/2}$ "No BU" cross section presents a pronounced CNI peak ($\sigma/\sigma_R \sim 1.4$) compared to the $2p_{3/2}$ "No BU" cross section ($\sigma/\sigma_R \sim 1.1$). In other words, the range of the projectile-target monopole nuclear interaction suppresses the CNI by approximately 22 %. It follows that the suppression of the CNI peak emanates from two main sources, strong coupling to the breakup channel and the long-range of the projectile-target monopole nuclear interaction.

In Fig. 4, we show how a high centrifugal barrier reduces the significance of the ground-state binding energy on the elastic scattering cross section. Panel (b) shows that the elastic scattering cross sections obtained for $S_n = -0.33$ MeV and $S_n = -0.15$ MeV are practically identical, which is a reflection of the ground-state densities in Fig. 1 (b). In panel (a), the smaller binding energy corresponds to a relatively lower scattering cross section, which would be expected by virtue of Fig. 1 (a).

The results in Figs. 2–3 have already shown that a high centrifugal barrier in the projectile ground-state strongly suppresses the breakup channel. To better dis-

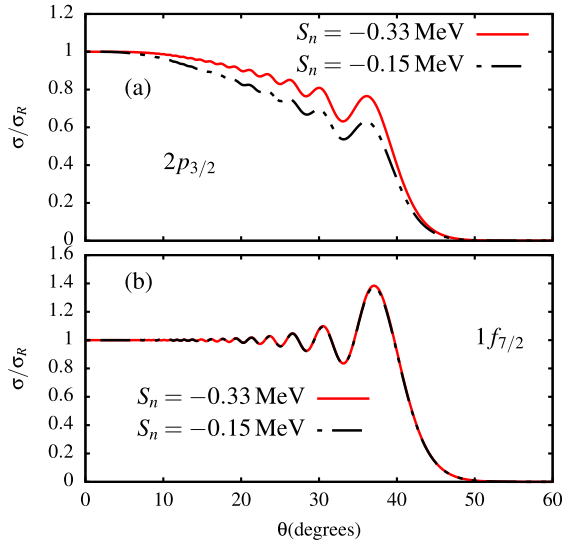


Fig. 4. (color online) Comparison of the elastic scattering cross sections corresponding to the $2p_{3/2}$ ground-state (panel (a)) and $1f_{7/2}$ ground-state (panel (b)) for $S_n = -0.33 \text{ MeV}$ and $S_n = -0.15 \text{ MeV}$.

play this fact, we consider the breakup cross sections. The differential angular-distribution breakup cross sections for $2p_{3/2}$ (panel (a)) and $1f_{7/2}$ (panel (b)) are shown in Fig. 5. Comparing the two breakup cross sections, it can be deduced that the peak of the $2p_{3/2}$ breakup cross section is approximately 130 orders of magnitude larger than that of the $1f_{7/2}$ breakup cross section. In other words, a higher ground-state orbital angular momentum corresponds to a very weak breakup channel, despite a low breakup threshold. One can infer that this parameter assimilates the breakup of a weakly-bound projectile to that of a tightly-bound projectile. Qualitatively, a higher centrifugal barrier in the projectile ground-state pushes the maximum of the breakup cross section at larger angles. For a better quantitative analysis, we summarize in Table 1 the integrated breakup cross sections (σ_{All}) for each ground-state configuration. As already noted in Fig. 5, the $1f_{7/2}$ breakup cross section is just a small fraction of its $2p_{3/2}$ counterpart. For example, for $S_n = -0.33 \text{ MeV}$, $\sigma(2p_{3/2}) \approx 46 \times \sigma(1f_{7/2})$, and $\sigma(2p_{3/2}) \approx 81 \times \sigma(1f_{7/2})$ for $S_n = -0.15 \text{ MeV}$. It is also shown that a high centrifugal barrier suppresses the quantitative effect of the binding energy on the breakup cross section.

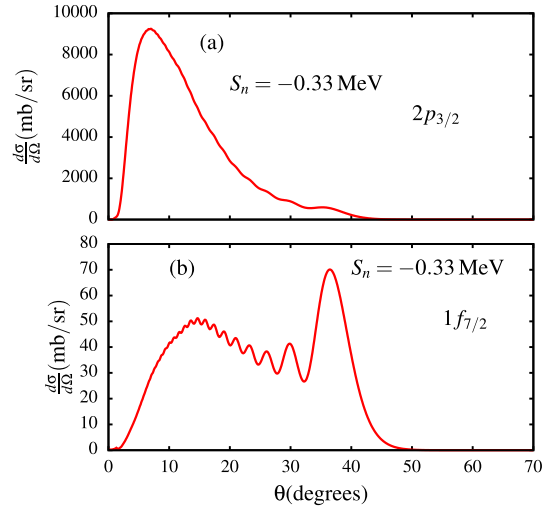


Fig. 5. (color online) Angular-distribution differential breakup cross sections corresponding to the $2p_{3/2}$ (panel (a)) and $1f_{7/2}$ (panel (b)) ground-states for $S_n = -0.33 \text{ MeV}$.

Table 1. Integrated breakup cross sections for the $2p_{3/2}$ and $1f_{7/2}$ ground-state configurations, corresponding to $S_n = -0.33 \text{ MeV}$ and $S_n = -0.15 \text{ MeV}$.

S_n/MeV	$2p_{3/2}$	$1f_{7/2}$	$\sigma(2p_{3/2})/\sigma(1f_{7/2})$
-0.33	3367	74	46
-0.15	8302	103	81

III. CONCLUSION

In this paper, an analysis of the breakup of the ^{31}Ne neutron-halo nucleus on a lead target, considering the $2p_{3/2}$ and $1f_{7/2}$ ground-state configurations, is presented. These two configurations provide an opportunity to investigate the relevance of a high ground-state centrifugal barrier on breakup dynamics. Considering the $2p_{3/2}$ ground-state, it is shown that couplings to the breakup channel suppress the CNI peak, as also reported in other works. However, no such suppression is obtained when considering the $1f_{7/2}$ ground-state. The reason is that a high centrifugal barrier almost wipes out the breakup channel and reduces the range of the monopole nuclear potential, which are two main factors that would otherwise suppress the CNI peak. The present study also identifies the couplings to the breakup channel and a long-ranged monopole nuclear potential as the leading factors in the suppression of the CNI peak.

References

- [1] I. Tain *et al.*, *Phys. Rev. Lett.* **55**, 2676 (1985)
- [2] V. Jha, V. V. Parkar, and S. Kailas, *Phys. Rep.* **845**, 1 (2020)
- [3] L. F. Canto, V. Guimarães, J. Lubian *et al.*, *Eur. Phys. J. A* **56**, 281 (2020)
- [4] B. Mukeru, T. Frederico, and L. Tomio, *Phys. Rev. C* **102**, 064623 (2020)
- [5] B. Mukeru, J. Lubian, and L. Tomio, *Phys. Rev. C* **105**, 024603 (2022)
- [6] J. Lei and A. M. Moro, *Phys. Rev. Lett.* **122**, 042503 (2019)

- [7] P. Capel, R. C. Johnson, and F. M. Nunes, *Eur. Phys. J. A* **56**, 300 (2020)
- [8] A. Pakou *et al.*, *Phys. Rev. C* **102**, 031601(R) (2020)
- [9] K.J. Cook *et al.*, *Phys. Rev. Lett.* **124**, 212503 (2020)
- [10] J. C. Zamora *et al.*, *Phys. Lett.B* **816**, 136256 (2021)
- [11] A. Di Pietro, A.M. Moro, J. Lei *et al.*, *Phys. Lett.B* **798**, 134954 (2019)
- [12] F.F. Duan *et al.*, *Phys. Lett.B* **811**, 135942 (2020)
- [13] R. Spartà *et al.*, *Phys. Lett. B* **820**, 136477 (2021)
- [14] K. Wang *et al.*, *Phys. Rev. C* **103**, 024606 (2021)
- [15] Y. Kucuk, V. Guimaraes, and B. V. Carlson, *Eur. Phys. J. A* **57**, 87 (2021)
- [16] D. Votaw *et al.*, *Phys. Rev. C* **102**, 014325 (2020)
- [17] B. Mukeru and L. Tomio, *Chin. Phys. C* **46**, 014103 (2022)
- [18] M. R. Cortes, J. Rangel, J. L. Ferreira *et al.*, *Phys. Rev. C* **102**, 064628 (2020)
- [19] M. Holl *et al.*, *Phys. Lett.B* **822**, 136710 (2021)
- [20] L. A. Souza, E. V. Chimanski, and B. V. Carlson, *Phys. Rev. C* **104**, 034623 (2021)
- [21] C. V. Midhun *et al.*, *Phys. Rev. C* **104**, 054606 (2021)
- [22] Y.L. Sun *et al.*, *Phys. Lett.B* **814**, 136072 (2021)
- [23] S. Watanabe, K. Ogata, and T. Matsumoto, *Phys. Rev. C* **103**, L031601 (2021)
- [24] K. Hagino, K. Ogata, and A.M. Moro, *Progr. Part. Nucl. Phys.* **125**, 103951 (2022)
- [25] N. Keeley, K. W. Kemper, I. Martel *et al.*, *Phys. Rev. C* **99**, 024603 (2019)
- [26] H. M. Maridi, K. Rusek, and N. Keeley, *Eur. Phys. J. A* **58** (2022)
- [27] B. Mukeru, *Int. Journ. Mod. Phys. E* **30**, 2150006 (2021)
- [28] B. Mukeru, L. V. Ndala, and M. L. Lekala, *Int. Journ. Mod. Phys. E* **31**, 2250025 (2022)
- [29] B. Mukeru, L. V. Ndala, and M. L. Lekala, *Pramana J. Phys.* **95**, 106 (2021)
- [30] B. Mukeru, L. V. Ndala, and M. L. Lekala, *Nucl. Phys. A* **1020**, 122397 (2022)
- [31] B. Mukeru, *J. Phys. Commun.* **5**, 075004 (2021)
- [32] B. Mukeru, M. L. Lekala, J. Lubian *et al.*, *Nucl. Phys. A* **996**, 121700 (2020)
- [33] V. Guimaraes *et al.*, *Eur. Phys. J. A* **57**, 90 (2021)
- [34] Yan Li and D. Y. Pang, *Eur. Phys. J. A* **57**, 46 (2021)
- [35] H. L. Crawford *et al.*, *Phys. Rev. Lett.* **122**, 052501 (2019)
- [36] X. N. Cao, Q. Liu, and J. Y. Guo, *Phys. Rev. C* **99**, 014309 (2019)
- [37] D. S. Ahn *et al.*, *Phys. Rev. Lett.* **123**, 212501 (2019)
- [38] S. Watanabe *et al.*, *Phys. Rev. C* **89**, 044610 (2014)
- [39] N. Kobayashi *et al.*, *Phys. Rev. Lett.* **112**, 242501 (2014)
- [40] I. Hamamoto, *Phys. Rev. C* **95**, 044325 (2017)
- [41] T. Nakamura *et al.*, *Phys. Rev. Lett.* **103**, 262501 (2009)
- [42] T. Nakamura *et al.*, *Phys. Rev. Lett.* **112**, 142501 (2014)
- [43] Y. Urata, K. Hagino, and H. Sagawa, *Phys. Rev. C* **83**, 041303(R) (2011)
- [44] W. Horiuchi, Y. Suzuki, P. Capel *et al.*, *Phys. Rev. C* **81**, 024606 (2010)
- [45] J. Hong, C. A. Bertulani, and A. T. Kruppa, *Phys. Rev. C* **96**, 064603 (2017)
- [46] I. Tanihata, H. Savajols, and R. Kanungo, *Prog. Part. Nucl. Phys.* **68**, 21 (2013)
- [47] P. Descouvemont, *Nucl. Phys. A* **655**, 440 (1999)
- [48] K. Minomo, T. Sumi, M. Kimura *et al.*, *Phys. Rev. C* **84**, 034602 (2011)
- [49] Shubhchintak and R. Chatterjee, *Nucl. Phys. A* **922**, 99 (2014)
- [50] A. Di Pietro *et al.*, *Phys. Rev. C* **85**, 054607 (2012)
- [51] Y.Y. Yang, X. Liu, and D.Y. Pang, *Phys. Rev. C* **94**, 034614 (2016)
- [52] L. Gaudefroy *et al.*, *Phys. Rev. Lett.* **109**, 202503 (2012)
- [53] B. Jurado *et al.*, *Phys. Lett.* **101**, 023210 (2007)
- [54] C. Ouellet and B. Singh, *Nucl. Data Sheets* **114**, 209 (2013)
- [55] G. Audi, A. H. Wapstra, and C. Thibault, *Nucl. Phys. A* **729**, 337 (2003)
- [56] N. Austern, *et al.*, *Phys. Rep.* **154**, 125 (1987)
- [57] Y. Iseri *et al.*, *Prog. Theor. Phys. Suppl.* **89**, 84 (1986)
- [58] I. J. Thompson and F. M. Nunes, *Nuclear Reactions for Astrophysics* (Cambridge University Press, New York, 2009).
- [59] R. O. Akyuz and A. Winther 1979 *Proc. Enrico Fermi Int. School of Physics, Nuclear structure and heavy-ion reactions*, ed. by R.A. Broglia, C.H. Dasso and R. Ricci (North-Holland, Amsterdam, 1981) p.491
- [60] I. J. Thompson, *Comput. Phys. Rep.* **7**, 167 (1988)
- [61] B. Mukeru, *Chin. Phys. C* **45**, 054107 (2021)
- [62] K. Riisager, A.S. Jensen, and P. Moller, *Nucl. Phys. A* **548**, 393 (1992)